In: Advances in Engineering Research. Volume 10 ISBN: 978-1-63482-784-3
Editor: Victoria M. Petrova

Chapter 3

INNOVATIVE PROCESS ENERGY SAVING BASED ON ENHANCED PROCESS INTEGRATION

Muhammad Aziz*, Takuya Oda and Takao Kashiwagi
International Research Center of Advanced Energy Systems for Sustainability,
Solutions Research Laboratory, Tokyo Institute of Technology,
Tokyo, Japan

ABSTRACT

This chapter discusses an innovative energy saving technology based on enhanced process integration (EPI). The discussion includes a theoretical study and application in industrial processes, especially those related to energy harvesting. EPI was developed based on two main core technologies: exergy recovery and process integration. First, exergy recovery focuses on the effective recirculation of energy or heat in the same process.

The idea of exergy recovery is different from that of conventional heat recovery. In exergy recovery, the quality of the recirculated energy is kept the same, and the recovered energy can thus be used as an energy source for a subsequent process. As a result, almost all energy involved in the process can be recirculated well, leading to minimization of exergy destruction. Furthermore, the proposed EPI technology was applied and evaluated in energy harvesting related processes and its performance was analyzed in term of energy efficiency. The proposed processes include the drying of low-rank coal, novel power generation from microalgae, and integrated power generation from empty fruit bunches. In the evaluated applications, the proposed processes showed high energy efficiency. Hence, their applications in real industrial processes are expected.

Keywords: exergy recovery, process integration, energy efficiency, exergy elevation, heat coupling

* E-mail: maziz@ssr.titech.ac.jp.

1. INTRODUCTION

Energy is critical to our daily lives. Our daily activities strongly depend on the way energy is generated (converted), transported, stored, and used. A high and fluctuating energy price and increased environmental awareness have changed the paradigm of energy use, especially in terms of energy conservation and the use of renewable energy resources. According to Zhu (2014), there are five ways to improve the energy efficiency in process industries: (1) minimize waste and loss, (2) optimize the process operation, (3) apply better heat recovery technology, (4) evaluate process changes, and (5) produce energy more efficiently.

Unfortunately, discussion on the improvement of energy efficiency in industrial processes has mainly focused on process intensification and integration alone. In addition, there has been no significant advance in heat recovery technologies. Conventional heat recovery technologies that were developed on the basis of pinch technology are limited in the sense that their heat exchange performance cannot be improved further. To solve this problem, enhanced process integration (EPI) was proposed to reduce exergy destruction both in a single process and in overall integrated processes.

This chapter discusses proposed EPI technology and covers both theoretical study and application in industrial processes. First, EPI is described theoretically as the combination of exergy recovery and process integration technologies. Furthermore, the application of EPI in some industrial processes, especially processes related to energy harvesting, are evaluated. The proposed innovative models include the drying of low-rank coal (LRC), power generation from microalgae through supercritical water gasification (SCWG) and a combined cycle, and energy harvesting from empty fruit bunches (EFBs).

2. PROPOSED EPI

2.1. Description of EPI

EPI was developed as the combination of its two core technologies: exergy recovery and process integration (Aziz et al., 2014a). This combination results in minimal total exergy destruction in the integrated processes. The exergy recovery deals with energy/heat circulation in a single process to recover effectively the energy involved in the same process (Aziz et al., 2015a). The concept of exergy recovery is different from that of conventional energy/heat recovery technology, such as pinch technology. Conventional heat recovery was developed according to the idea of heat cascade utilization, which mainly focuses on the temperature without further consideration of how to minimize the waste heat that cannot be recovered owing to the limitation of the minimum temperature approach (pinch). In exergy recovery, in contrast to conventional heat recovery, all the energy/heat involved is basically recirculated. The limitation of the minimum temperature approach is not considered a main issue in exergy recovery.

The idea stems from thorough heat circulation. Figure 1(a) shows the basic principle of exergy recovery for a simple process involving heating, evaporation, and superheating. Solid and dotted lines represent hot and cold streams, respectively.

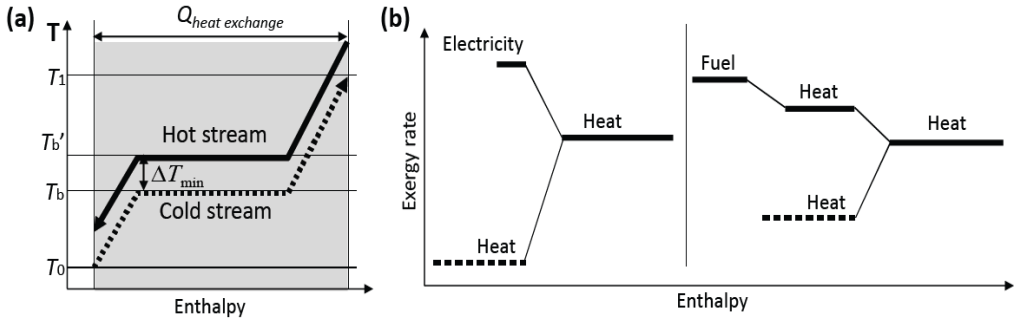

Figure 1. Principle of exergy recovery: (a) basic concept of exergy recovery, (b) two examples of how to elevate the exergy rate.

Basically, exergy can be recovered through exergy elevation and heat coupling of the hot and cold streams. After a certain process ends, the exergy of the process stream (cold stream) is elevated to a certain exergy rate, creating a hot stream. Furthermore, the elevation of exergy depends strongly on the performance of the heat coupling between the hot stream and cold stream afterward. This exergy elevation becomes a key factor distinguishing the proposed exergy recovery and conventional heat recovery (Liu et al., 2012a).

Exergy can be elevated using available methods that employ, for example, compression, the combination of heat having different exergy rates, and the magnetocaloric effect (Kotani et al., 2013; Liu et al., 2014). Figure 1(b) shows two simplified examples of how to elevate the exergy rate of the process stream. On the left side, the exergy of the cold stream is elevated through compression that uses electricity as the energy input. By applying compression, the pressure and temperature of the cold stream (compressible stream) rise. Hence, physical properties, such as the saturation point, of the stream change accordingly. On the right side, the exergy rate of the cold stream is elevated by combination with another stream having a higher exergy rate (temperature) that might be produced from chemical energy (fuel). This combination includes the direct mixing and heating of streams through heat exchange.

After the exergy elevation, the hot stream is used as the heat source for the subsequent process through effective heat coupling. In the case of exergy elevation through compression, as the saturation point of the stream changes, heat coupling is performed by considering the pairing of the same type of heat including latent and sensible heat. As a result, the optimum balance of heat can be achieved, leading to minimum exergy destruction or wasted heat throughout the process. This can be observed from the temperature–enthalpy diagram in which the curves of both hot and cold streams are almost parallel to each other.

Unfortunately, for reasons including the use of the minimum temperature approach and changes in chemical and physical properties, there can be an imbalance of heat leading to unrecoverable heat in a certain process. As an example, when a stream is compressed, the amount of latent heat of the stream decreases, leading to inequality when the stream is paired with a cold stream in the same process. To minimize this exergy destruction, the idea of process integration is adopted. The unrecoverable heat in a certain single process is used in other processes leading to further minimization of total exergy destruction in the overall integrated processes. As a result, the total energy loss can be minimized, leading to higher energy efficiency.

2.2. Basic Tools for Analysis

Energy analysis is usually performed by modeling balances of mass, energy, and exergy. In a steady state with no heat loss from the system, the mass, energy, and exergy balances are generally written as

$$\sum_i m_{\mathrm{in},i} = \sum_e m_{\mathrm{out},e} \,, \tag{1}$$

$$\sum_i m_{\mathrm{in},i}\ h_{\mathrm{in},i} = \sum_e m_{\mathrm{out},e}\ h_{\mathrm{out},e} + W \tag{2}$$

$$\sum_i m_{\mathrm{in},i}\ ex_{\mathrm{in},i} = \sum_e m_{\mathrm{out},e}\ ex_{\mathrm{out},e} + W + \sum_j Ex_{des,j} \,, \tag{3}$$

where m, h, W, ex, and Ex are the mass, specific enthalpy, mechanical or electrical work, specific exergy, and exergy, respectively.

Exergy relates strongly to the second law of thermodynamics on irreversibility due to increase of entropy. Hence, exergy is not conserved. The total exergy can be calculated as the sum of physical exergy, ex_{ph}, and chemical exergy, ex_{ch}, which are calculated as

$$ex = ex_{ph} + ex_{ch} \,, \tag{4}$$

$$ex_{ph} = (h - h_0) - T_0\,(s - s_0) \,, \tag{5}$$

$$h - h_0 = \int_{T_0}^{T} C_{\mathrm{p}}\ \mathrm{d}T \,, \tag{6}$$

$$s - s_0 = \int_{T_0}^{T} \frac{C_{\mathrm{p}}}{T}\ \mathrm{d}T \,, \tag{7}$$

$$ex_{ch} = \sum_i x_i \left[ex_{ch,i} + RT_0 \ln\left(x_i \Big/ \sum x_i \right) \right] , \tag{8}$$

where T, Cp, s, x, and R are temperature, heat capacity, specific entropy, molar fraction, and universal gas constant, respectively.

Exergy destruction due to irreversibility can occur because of processes such as heat exchange, compression, and conversion. Exergy can be divided into inevitable exergy and avoidable exergy (Aziz et al., 2014b; Liu et al., 2012b). The inevitable exergy is defined as the minimum exergy destruction that is required for a process or reaction to take place. Avoidable exergy loss relates to exergy destruction due to a surrounding process that supports

the progression of the main process or reaction, such as heat exchange and compression (Liu et al., 2013). This chapter deals with avoidable exergy, specifically the minimization of exergy destruction through EPI. The following are representative examples of exergy destruction.

a. Exergy destruction during heat exchange

$$Ex_{\mathrm{des,HX}} = Ex_{\mathrm{hot,in}} + Ex_{\mathrm{cold,in}} - Ex_{\mathrm{hot,out}} - Ex_{\mathrm{cold,out}} \quad (9)$$

b. Exergy destruction following compression

$$Ex_{\mathrm{des,cp}} = Ex_{\mathrm{in}} - Ex_{\mathrm{out}} + W_{\mathrm{cp}} \quad (10)$$

c. Exergy destruction in combustion

$$Ex_{\mathrm{des,comb}} = Ex_{\mathrm{in}} - Ex_{\mathrm{out}} + Ex_{\mathrm{fuel}} \quad (11)$$

3. ENERGY-EFFICIENT DRYING OF LOW-RANK COAL

3.1. Introduction

Low-rank coal (LRC), specifically brown and sub-bituminous coals, account for more than 50% of the world's coal resources (Aziz et al., 2011). The production of LRC has increased owing to the energy crisis and high oil prices. Compared with coals of higher rank, LRC has beneficial characteristics including lower sulfur content, higher reactivity, and lower mining cost due to the possibility of open-cut mining. Unfortunately, LRC has the disadvantages of a high moisture content, low calorific value, high risk of spontaneous combustion, and high CO_2 emissions. The high moisture content of LRC results in a low calorific value, high transportation cost, unstable storage, and difficult handling in loading and unloading (Aziz et al., 2012a). To overcome these problems, pretreatment such as the drying of LRC before use is necessary. By reducing the moisture content, LRC can be used more broadly, such as in gasification, pyrolysis, liquefaction, and briquetting.

Drying is one of the most energy-intensive industrial processes. To improve the energy efficiency, conventional methods of drying—pinch, heat pump, and vapor recompression technologies—have recently been developed (Aziz et al., 2014b). However, these conventional processes cannot substantially recover the energy involved in drying owing to large exergy destruction. As a result, large energy input for drying is required. To minimize the energy input in the drying of LRC, an innovative drying method based on EPI was proposed and evaluated.

3.2. Proposed Energy-Efficient LRC Drying

Figure 2 is a schematic diagram showing the process flow of the proposed drying process based on EPI, especially exergy recovery applying both exergy elevation and heat coupling.

Superheated steam is adopted as the drying medium because of its advantages of higher heat capacity, higher thermal efficiency, faster drying, and lower fire and explosion risks. The as-mined LRC is initially ground to obtain LRC particles of uniform and small size resulting in larger surface area for heat exchange and evaporation and better transportation/handling during drying. Next, the ground LRC enters preheater 1 for preheating using the heat from the condensed compressed steam.

The preheated LRC then flows to the main dryer for water evaporation. A rotary dryer with immersed heating tubes is selected as the dryer to facilitate effective heat coupling. The advantages of the steam tube rotary dryer include a large heat transfer surface area, excellent drying control, easy handling, and the possibility of continuous operation (Devahastin and Mujumdar, 2007). Additionally, to minimize the temperature, heat exchange between hot and cold streams inside the rotary dryer is designed as a counter-current. The rotary dryer has a sloping rotating cylinder in which LRC particles move naturally from the inlet to outlet under the force of gravity. Further, the heating tubes are arranged in concentric circles inside the rotary dryer and rotate together with the rotary dryer (Aziz et al., 2014b). The compressed steam flows inside these heating tubes and provides the heat source for drying. The main goal is latent heat exchange between the condensation heat of compressed steam and evaporation heat of water within LRC. The water evaporated from LRC flows from the outlet and enters the cyclone for separation. The exhausted steam is then separated as recirculated steam and purged steam. The recirculated steam is used as the drying medium inside the rotary dryer to improve the distribution of heat transfer and material agitation. In addition, the existence of recirculated steam reduces the fire risk during drying owing to the high heat capacity of steam.

The amount of recirculated steam is constant throughout drying. The purged steam, which originates from the water that evaporated from the LRC, flows to the compressor for exergy elevation. The heat exchange inside the dryer occurs in two ways: convective heat transfer (from the recirculated steam) and conductive heat transfer (from the compressed steam in the heating tubes).

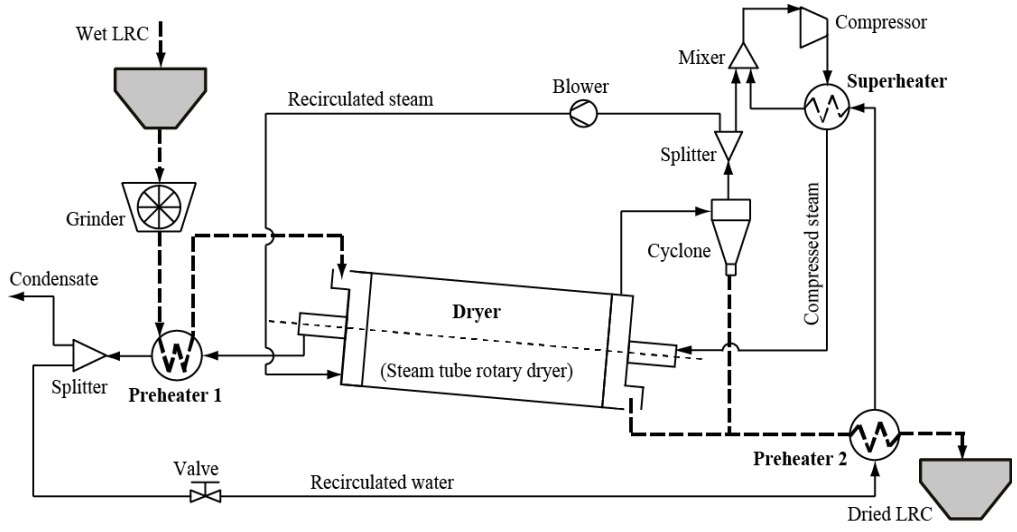

Figure 2. Process flow diagram of the proposed drying of LRC based on EPI.

Through compression, the physical properties of steam change and the saturation point increases. The amount of compression depends strongly on the heat exchange performance throughout the process. The energy that can be earned from the compressed steam and used for drying is greater than the electricity input for compression. The adiabatic compression work, W_{cp}, can be defined as

$$W_{cp} = \frac{\kappa}{\kappa - 1} p_{suc} v_{suc} \left\{ \left(\frac{p_{dis}}{p_{suc}} \right)^{(\kappa-1)/\kappa} - 1 \right\}, \tag{12}$$

$$v_{suc} = v_{boil} \left(\frac{p_{boil}}{p_{suc}} \right) \left(\frac{T_{suc}}{T_{boil}} \right), \tag{13}$$

where κ, p_{suc}, p_{dis}, v_{suc}, v_{boil}, T_{suc}, and T_{boil} are the heat capacity ratio, suction pressure, discharge pressure, specific volume at the suction temperature, specific volume at the boiling temperature, suction temperature, and boiling temperature, respectively.

The dried LRC particles are discharged from the outlet on the bottom side. To recover the heat of the dried LRC, part of the condensate from preheater 1 is recirculated and heated in preheater 2. The condensate then flows to the superheater for both evaporation and superheating and mixes with the purged steam before entering the compressor. This mixing improves the material balance in the hot stream and lowers the pressure ratio during compression. It is important to note that, for the same stream, as the pressure increases, the latent heat decreases. Hence, the latent heat cannot be paired equally. In addition, in the rotary dryer, the heat exchange involves not only the latent heat of water but also the sensible heat of LRC solid. The compressed steam then flows back to the superheater, rotary dryer, and preheater 1, continuously. The steam condenses during drying and is exhausted as condensate from preheater 1. It is important to pair the same type of heat to achieve an optimal balance of heat and thus optimize optimal heat coupling.

In thermophysical drying, the equilibrium moisture content is strongly affected by the temperature, humidity, and pressure of the surrounding environment. Furthermore, in the case of drying with superheated steam, the equilibrium moisture content is affected by the relative vapor pressure. The relation between the relative vapor pressure and equilibrium moisture content of LRC can be calculated as (Chen et al., 2001)

$$\frac{p}{p_{sat}} = 1 - \exp\left[-2.53 \left(T_{dry} - 273 \right)^{0.47} \left(MC \middle/ \left(100 - MC \right) \right)^{1.58} \right] \tag{14}$$

where p_{sat}, T_{dry}, and MC are the saturation pressure, drying temperature, and equilibrium moisture content, respectively.

The proposed LRC drying process was evaluated under the following conditions; (1) a rotary dryer with immersed heating tubes is modeled as a mixer, heat exchanger, and separator, (2) the minimum temperature is 15 K, (3) the flow rate of wet LRC is 100 t h^{-1}, (4)

the initial moisture content of wet LRC is 50 wt% wb, (5) target moisture contents are set to 5, 10, and 15 wt% wb, and (6) the ambient pressure and temperature are 101.33 kPa and 25 °C, respectively. The process modeling and calculation were conducted using the Pro/II steady-state process simulator (Invensys Corp.). Table 1 gives the properties of LRC used in the evaluation. The heat transfer inside the rotary dryer is approximated as

$$\frac{1}{UA} = \frac{1}{A_c \alpha_c} + \frac{\ln\left(R/r\right)}{2\pi L \lambda_t} + \frac{1}{\alpha_t A_t}, \tag{15}$$

where U, A, A_c, α_c, λ_t, r, R, α_t, and A_t are the total heat transfer coefficient, total surface area for heat exchange, inner surface area of heating tubes, heat transfer coefficient following two-phase condensation, thermal conductivity of heating tubes, inner and outer radii of heating tubes, convective heat transfer coefficient, and outer surface area of heating tubes, respectively.

Table 1. Properties of LRC used in evaluation

Property	Value
Type	Sumatera brown coal
Ash (wt.% db)	6.39
Carbon C (wt.% db)	64.06
Hydrogen H (wt.% db)	4.54
Nitrogen N (wt.% db)	0.26
Sulfur S (wt.% db)	0.25
Oxygen O (wt.% db)	24.5
Calorific value (MJ/kg)	21.3

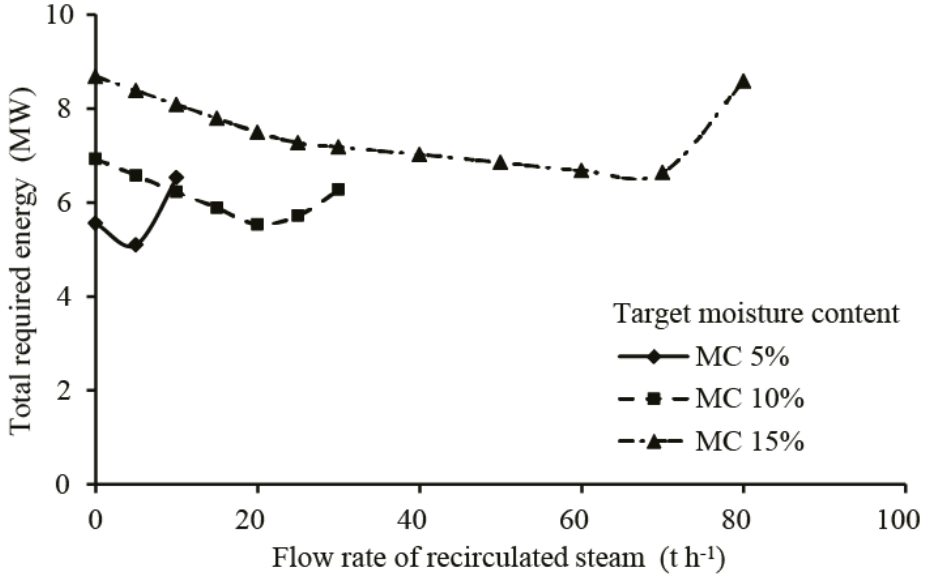

Figure 3. Correlation between the flow rate of recirculated water and total energy required for drying.

Figure 3 shows the relation between the flow rate of recirculated steam and the total energy input required for LRC drying. The total required energy is defined as the total work consumed in the compressor, blower, and driving motor. Drying to a lower moisture content results in lower total energy input because of a larger amount of evaporated water and better material balance can be achieved, leading to more effective heat coupling. This leads to lower compression work, which is the largest work component during drying. Furthermore, there is an optimum flow rate of recirculated steam for each target moisture content. A lower target moisture content requires a smaller amount of recirculated steam.

To achieve a relatively high gasification temperature and boiler efficiency, LRC needs to be dried to a moisture content of about 10 wt% wb (Hu et al., 2013). However, a very low moisture content poses a higher fire risk related to a lower critical ignition temperature. Hence, drying to a moisture content of 10 wt% wb is considered the most appropriate drying condition for LRC in terms of efficiency, safety, and energy consumption.

Figure 4 is a temperature–enthalpy diagram of the proposed LRC drying. Solid and dotted lines represent hot and cold streams, respectively. The heat exchange is largest in the rotary dryer in which latent heat exchange between the condensation heat of compressed steam and evaporation heat of water from LRC occurs. Heat is also largely exchanged in the superheater between the compressed steam and condensate. The curves of hot and cold streams are almost completely parallel to each other. This means that effective heat coupling between the streams can be achieved, leading to a minimum amount of wasted energy; i.e., exergy destruction.

4. INTEGRATED ENERGY HARVESTING FROM MICROALGAE

4.1. Introduction

Microalgae are considered a potential energy resource. Compared with terrestrial crops, microalgae have a higher growth rate, are more efficient in absorbing CO_2, and can grow even in a severe environment that is not suitable for terrestrial crops (Hu et al., 2014; Aziz et al., 2012b).

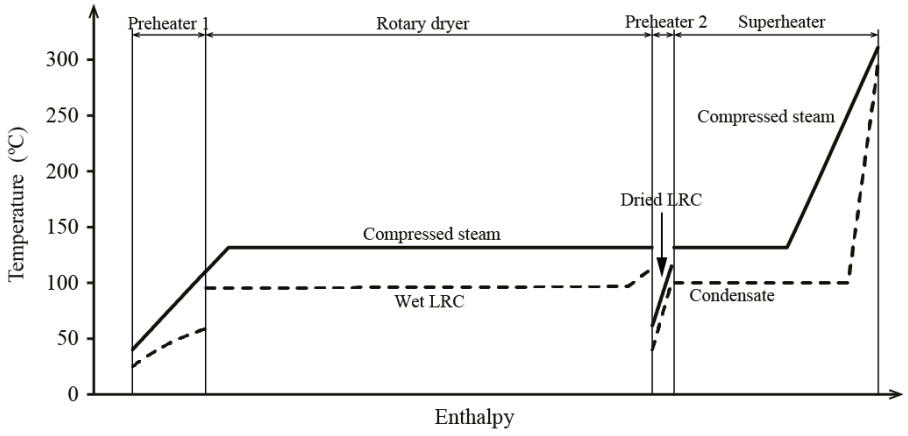

Figure 4. Temperature–enthalpy diagram of the proposed LRC drying.

Microalgae effectively convert sunlight to chemical energy through photosynthesis. In addition, their ability to absorb CO_2 effectively suggests their possible use in the bio-sequestration of emitted CO_2. The combination of the use of microalgae as an energy resource and the use of microalgae in the bio-sequestration of CO_2 would lead to clean energy production, especially for power generation. Moreover, the calorific value of dried microalgae is relatively high (19–25 GJ t^{-1}) and comparable to that of sub-bituminous coal (Mc Ginn et al., 2011).

Unfortunately, microalgae have very high moisture content, ranging from 70 to 90 wt% wb, making their use difficult. Drying is an energy-intensive process, especially owing to the latent heat of water evaporation. Currently, energy harvesting from microalgae is very inefficient, leading to negative energy performance (the energy input required for overall conversion is greater than the energy that can be produced). In addition, to harvest energy, microalgae can be converted through thermochemical and biochemical processes. Generally, thermochemical processes are advantageous owing to their faster conversion time and more complete conversion products. These processes include gasification, pyrolysis, and liquefaction. Unfortunately, in the conventional thermochemical process, the harvested microalgae must be dried to relatively low moisture content to facilitate the process to progress well.

The best method of avoiding the above problems is considered to be the conversion of microalgae in their aqueous phase in terms of total energy efficiency as the avoidance of drying. Hence, SCWG is adopted to convert microalgae to syngas. The produced syngas is then used as a fuel for power generation through a combined cycle. In-situ energy conversion through integrated processes is considered the best method of harvesting energy from microalgae. The generated electricity can be delivered through an electricity grid as a cheaper transportation method. Hence, higher total economic performance and feasibility can be achieved.

4.2. Integrated SCWG and Combined Cycle

The integration of energy harvesting from microalgae is based on the idea of material and energy circulation including cultivation, conversion, and power generation. In cultivation, microalgae are grown in an aqueous environment absorbing the surrounding nutrients and sunlight (Aziz et al., 2014c). The harvested microalgae are converted as a fuel through SCWG and the unconverted materials can be recirculated as nutrients for cultivation. Next, the fuel is used for power generation employing a combined cycle. The exhausted flue gas, which is rich in CO_2, is also recirculated in cultivation for its heat and chemical compounds.

SCWG thermocally converts microalgae to syngas by applying the advantages of supercritical water properties. Although SCWG can bypass drying, the energy required to bring the microalgae to a supercritical condition (minimum pressure and temperature of 22.1 MPa and 374 °C, respectively) is relatively high. Hence, a further measure is urgently required to improve the total efficiency. In SCWG, water acts as a solvent and its density decreases as the pressure exceeds the critical point (Kruse, 2008). The static relative dielectric constant, hydrogen bonding, and polarity of water reduce beyond the critical point (Haiduc et al., 2009). In addition, under a supercritical condition, water has good transport properties.

Hence, the reaction can be performed in a single homogeneous phase of fluid resulting in the easier conversion of hydrocarbons and carbohydrates.

Figure 5 is a process flow diagram of the proposed integration of SCWG and the combined cycle for microalgae. Microalgal slurry is pumped to a supercritical pressure and then preheated before entering the gasifier (SCWG reactor). Water is also pumped and preheated before being used as a fluidizing medium. In the gasifier, microalgae are converted to syngas containing CO, H_2, and CH_4. The exhausted syngas and steam flow to the superheater for exergy elevation. In this case, the exergy is elevated through heat exchange using the higher temperature of the heat source, which is flue gas from the gas turbine. The purpose of this exergy elevation is to realize a self-heat exchange during gasification. Hence, a fluidized bed with an immersed heat exchanger is adopted to facilitate the self-heat exchange. In addition, a fluidized bed can avoid plugging during gasification (Matsumura and Minowa, 2004).

After superheating, syngas and steam flow back through the heat exchanger inside the gasifier. There is a large amount of heat exchange between the microalgae and superheated mixture of syngas and steam during gasification. The condensed mixture of syngas and steam discharged from the gasifier flows to preheaters as a heat source and is finally separated to produce pure syngas. The produced syngas is used for fuel and combusted under high pressure to produce an effective torque that rotates the gas turbine for power generation.

Furthermore, the flue gas from the gas turbine is used as a heat source for superheating before its remaining heat is recovered in the heat recovery steam generator (HRSG) to generate steam for the steam turbine.

To evalute the performance of the integrated SCWG and combined cycle, process modeling and calculations using *Spirulina* sp. as biomaterial were conducted. *Spirulina* has a high lipid content and affinity to water leading to more efficient conversion during gasification (Venkitasamy et al., 2011). Table 2 presents the ultimate analysis of *Spirulina*, gasification conditions, and combined cycle specifications.

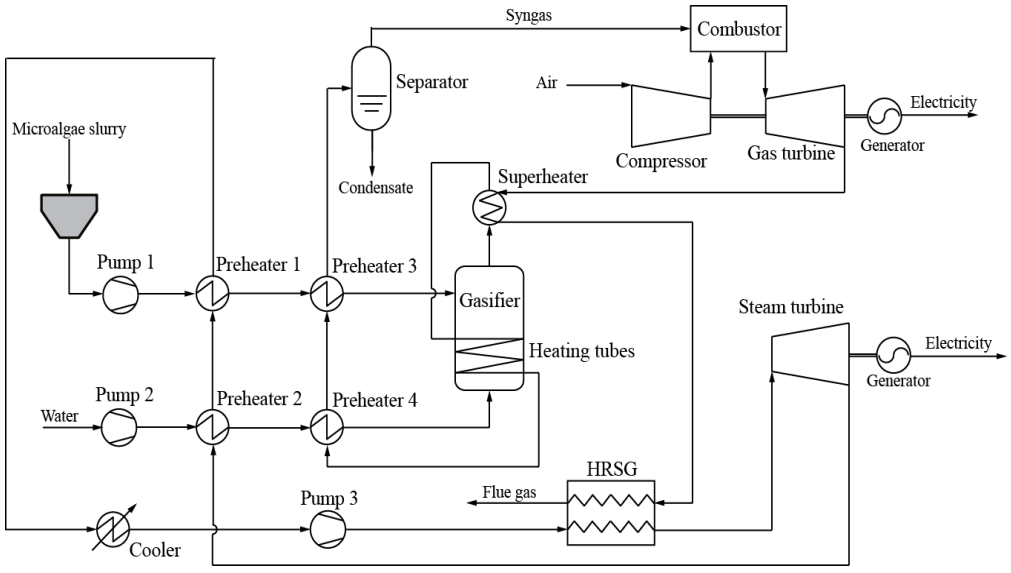

Figure 5. Basic process flow diagram of the integrated SCWG and combined cycle for microalgae.

Table 2. Ultimate analysis of *Spirulina*, SCWG conditions, and combined cycle specifications

Properties	Values
Ultimate analysis (Chaiwong et al., 2012)	
Carbon (wt.% db)	42.83
Hydrogen (wt.% db)	6.02
Nitrogen (wt.% db)	4.09
Sulfur (wt.% db)	0.49
Oxygen (wt.% db)	46.57
Gasification products (Chakinala et al., 2010)	
CO (dry mol%)	3.1
C_2H_6 and C_3H_8 (dry mol%)	4.9
CH_4 (dry mol%)	18.1
CO_2 (dry mol%)	27.8
H_2(dry mol%)	46.1
Gasification conditions	
Fluidization velocity U/U_{mf} (-)	1, 2, 3, 4
SCWG pressure (MPa)	22, 25, 28, 30
SCWG temperature (°C)	700
Carbon conversion efficiency (%)	100
Alumina particles diameter (mm)	0.3
Combined cycle	
Gas turbine inlet temperature (°C)	1300, 1500
Compressor outlet pressure (MPa)	2
Gas turbine adiabatic efficiency (%)	90
HRSG outlet pressure (MPa)	20
Steam turbine polytrophic efficiency (%)	90
Minimum outlet vapor quality (%)	90

In addition, general assumptions were made: (1) the flow rate of wet *Spirulina* is 1000 t h^{-1}, (2) the minimum temperature in all heat exchangers is 10°C, (3) the SCWG gasifier comprises a mixer, heat exchanger, Gibbs reactor, and separator, and (4) Ru/TiO_2 is used as the catalyst for gasification with a catalyst-to-microalgae weight ratio of 2.

The pressure drop across the gasifer, Δp, is approximated as

$$\frac{\Delta p}{H} = 150\frac{(1-\varepsilon)^2}{\varepsilon^3}\times\frac{\mu_g U_g}{(\varphi_p\, d_p)^2} + 1.75\frac{1-\varepsilon}{\varepsilon^3}\times\frac{\rho_g {U_g}^2}{\varphi_p\, d_p} \tag{16}$$

where H, ε, μ, U, ρ, φ, and d are the height, fraction, dynamic viscosity, velocity, density, sphericity, and diameter, respectively.

The minimum fluidization velocity, U_{mf}, during gasification is estimated according to (Lu et al., 2013)

$$Re_{\mathrm{mf}} = \frac{\rho_{\mathrm{g}} U_{\mathrm{mf}} d_{\mathrm{p}}}{\mu_{\mathrm{g}}}, \tag{17}$$

$$Re_{\mathrm{mf}} = \left(27.3^2 + 0.0434\, Ar\right)^{0.5} - 27.3, \tag{18}$$

$$Ar = \frac{d_p^3\, \rho_{\mathrm{g}} \left(\rho_{\mathrm{p}} - \rho_{\mathrm{g}}\right) g}{\mu_g^{\,2}}, \tag{19}$$

where Re_{mf}, Ar, ρ_{p}, ρ_{g}, d_{p}, μ_{g}, and g are the Reynolds number at minimum fluidization velocity, Archimedes number, particle density, gas density, gas dynamic viscosity, and acceleration due to gravity, respectively.

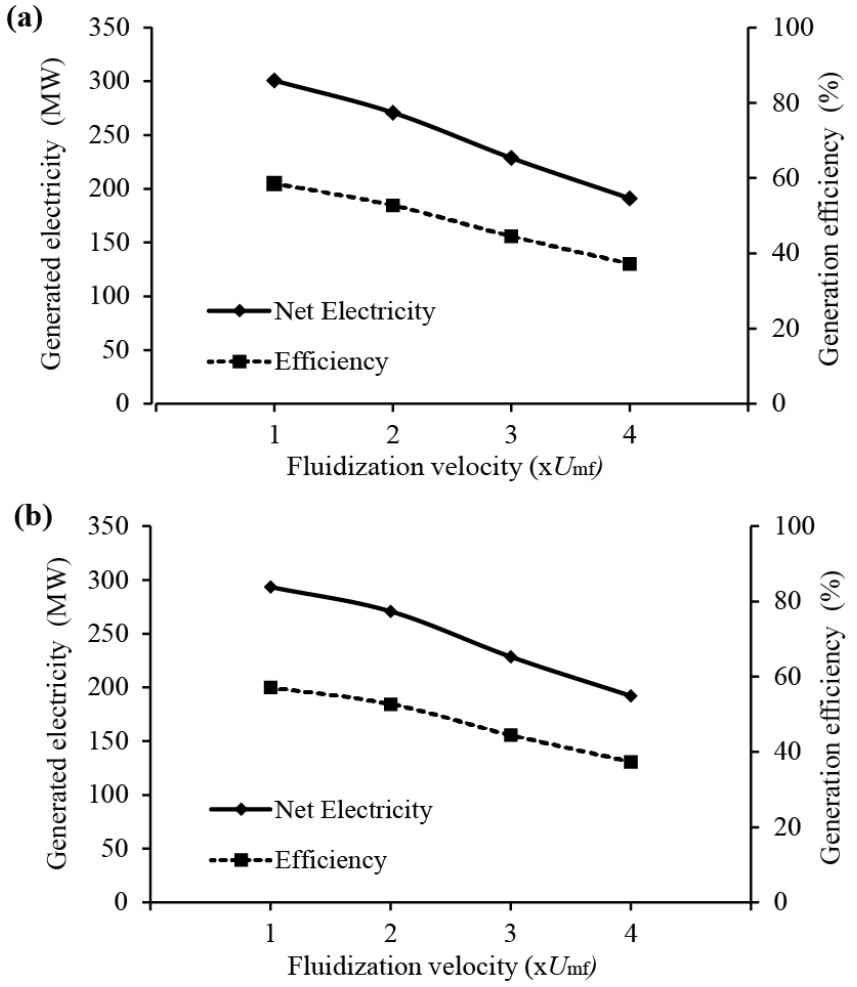

Figure 6. Effect of the fluidization velocity on the generation of electricity and generation efficiency (SCWG pressure of 25 MPa): (a) turbine inlet temperature of 1500°C, (b) turbine inlet temperature of 1300°C.

Figure 6 shows the correlation among fluidization velocity, generated electricity, and generation efficiency at different turbine inlet temperatures (where the SCWG pressure is fixed at 25 MPa). Generally, the total generation efficiency is relatively high, higher than 35% under all evaluated conditions. There is no marked increase in generated electricity and generation efficiency when the turbine inlet temperature is raised from 1300 to 1500°C. A higher turbine inlet temperature results in more exergy, which is further recovered by gas and steam turbines. In addition, the generated electricity and generation efficiency decrease following an increase in the fluidization velocity. As the fluidization velocity increases, the heat consumed to elevate the temperature of syngas and steam during superheating increases. As a result, the energy available to generate steam for the steam turbine decreases (Aziz, 2015a). In the case of a fluidization velocity of 1 U_{mf}, the generated electricity is about 300 MW and the generation efficiency is about 58%. According to these results, employing the proposed integrated processes of the SCWG and combined cycle, the generation of power from microalgae can achieve very high energy efficiency.

Figure 7 shows the effect of the SCWG pressure on the generated electricity and generation efficiency for a fluidization velocity and turbine inlet temperature of 2 U_{mf} and 1500°C, respectively. There was no marked change in either the generated electricity or generation efficiency although the SCWG pressure increased from 22 to 30 MPa.

However, the generated electricity, as well as the generation efficiency, decreased following an increase in SCWG pressure. The main cause is considered to be the change in density of fluid (steam) due to the change in pressure. As a result, higher SCWG pressure leads to a larger amount of steam required for fluidization owing to the increase in density. Hence, the work required to pump the water increases. In addition, as the amount of fluidizing steam increases, the heat required for superheating also increases, leading to more consumed energy in superheating. Ultimately, there is less energy available to be recovered by the steam turbine.

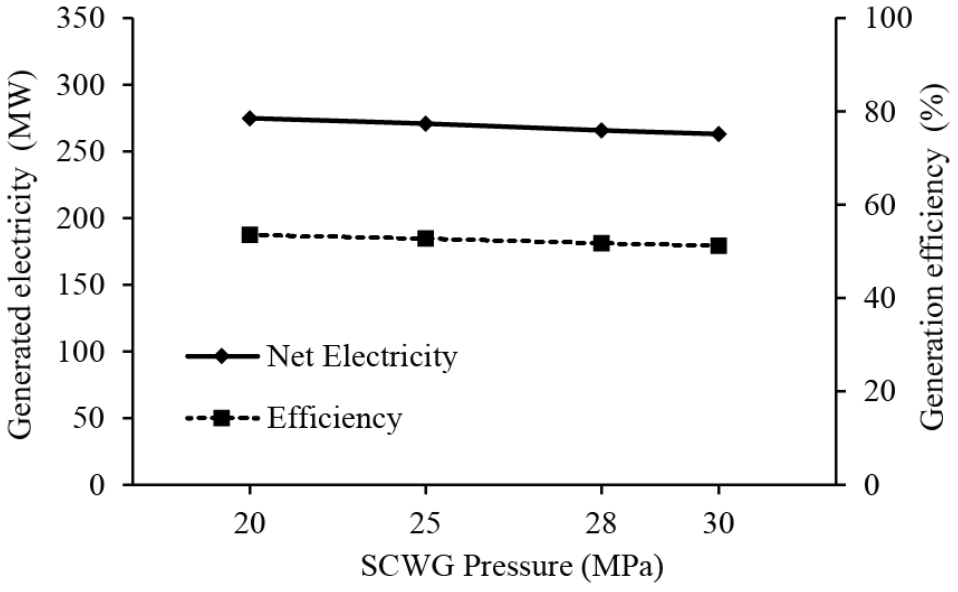

Figure 7. Effect of SCWG pressure on the generated electricity and generation efficiency (turbine inlet temperature and fluidization velocity are 1500°C and 2 U_{mf}, respectively).

5. NOVEL POWER GENERATION FROM EFBS

5.1. Introduction

The demand for palm oil and its products is increasing rapidly following global economic growth. Palm oil is a vegetable oil harvested from the palm tree (*Elaeis guianeensis*). The increase demand for palm oil has raised serious environmental problems owing to huge amounts of wastes, including EFBs, fibers, and shells (Aziz et al., 2015c). In addition, palm oil production only involves about 10% of the whole palm tree and the remainder is abandoned or recycled back to cultivation (Thong et al., 2012).

Among the solid wastes, EFBs have the lowest economic value owing to their high moisture content and need for additional pretreatment before use. The quantity of EFBs generated from fresh fruit bunches during palm oil production is about 20% (Kerdsuwan and Laohalidanond, 2011). EFBs have the characteristics of a high moisture content (60–70 wt% wb), low bulk density, and nonuniform shape (Paepatung et al., 2009). There is an urgent demand for the innovative use of EFBs to increase the economic value of EFBs and to reduce environmental problems.

One potential use of EFBs is as energy resource. Unfortunately, there has been very little research on the innovative use of EFBs as an energy resource with relatively high energy efficiency. A novel use of EFBs as energy resource for power generation has been proposed by Aziz et al. (2015b). The proposed integrated processes based on EPI include drying, gasification, and a combined cycle.

5.2. Proposed Integrated Processes

In general, the proposed integrated processes cover pretreatment (drying), conversion (gasification), and power generation (combined cycle). Figure 8 is a schematic diagram of the process flow of the proposed integrated processes for power generation from EFBs developed based on EPI. In drying, superheated steam is adopted as the drying medium. Raw and wet EFBs are initially pretreated by cutting and shredding to achieve smaller and uniform size. EFBs are then preheated using the condensate compressed steam and flue gas from the gas turbine and HRSG.

Next, the EFBs flow to the dryer for moisture removal. A fluidized-bed-type dryer is adopted to dry the EFBs owing to its uniform temperature distribution, excellent particle mixing, and rapid heat transfer.

In addition, to facilitate effective heat coupling, heating tubes are immersed inside the bed and steam is blown from the bottom for fluidization. To improve the fluidization of EFB particles and achieve uniform heat transfer across the bed, silica sand is used as the fluidizing medium.

The evaporated water is exhausted from the dryer and separated to recirculated and purged (compressed) steams. The recirculated steam is basically constant in its flow rate and used as a fluidizing gas to facilitate a uniform heat and moisture transfer across the bed. Conversely, the purged steam is compressed by a compressor and is recirculated back to the dryer through heating tubes. It is mainly used to provide a heat source for subsequent drying.

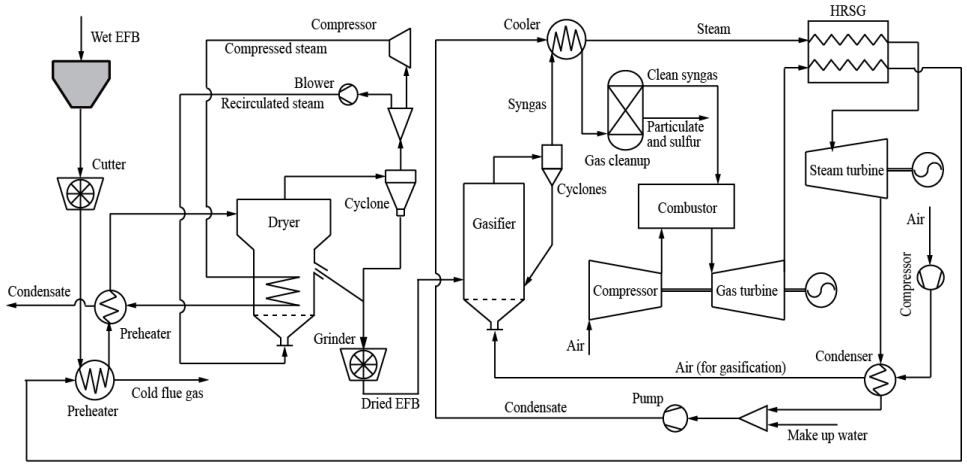

Figure 8. Schematic diagram of the integrated power generation system for EFBs covering drying, gasification, and combined cycle.

In the fluidized bed, latent heat exchange occurs predominantly between the condensation heat of the compressed steam and evaporation heat of water originating from the EFBs. As its heat dissipates, the compressed steam condenses and flows out from heating tubes flowing to the preheater to preheat the wet EFBs.

The dried EFBs, which have lower density, are segregated during fluidization and discharged from the dryer by overflow. The material is then ground to achieve a smaller size before entering the gasifier. Air gasification is adopted on the basis of the experimental reports of Mohammed et al. (2012). A gasifier with a fluidized bed as a reactor is adopted in this study. During gasification, EFB material is converted to syngas that is rich in CO, H_2, and CH_4. The produced syngas is cooled for heat recovery and cleaned to produce clean syngas.

This clean syngas is used as fuel for combustion under high pressure to create a gas of high pressure and temperature to rotate the gas turbine. The flue gas from gas turbine is then recovered in the HRSG, generating steam for the steam turbine.

Table 3 presents the elemental analysis of EFBs and the conditions of drying, gasification, and the combined cycle used in this study. General assumptions made were (1) the flow rate of raw wt EFB is 100 t h^{-1}, (2) the fluidized bed gasifier consists of a mixer and a conversion reactor, (3) the minimum temperature in the dryer and other heat exchangers is 10°C and 20°C, respectively, (4) air contains 79% nitrogen and 21% oxygen and has relative humidity of 60%, and (5) initial and target moisture contents of EFB are 60 wt% wb and 5 wt% wb, respectively. The modeling and calculation were performed using a Pro/II steady-state process simulator (Invensys Corp.).

The effect of three gasification temperatures was analyzed. Table 4 shows the relation between the gasification temperature and produced syngas composition (Mohammed et al., 2011).

Generally, the gasification yield and its total lower heating value (LHV) increase as the gasification temperature increases from 800 to 1000°C. In addition, the water–gas shift reaction and thermal cracking progress better under higher gasification temperature. The equilibrium moisture content for EFBs under superheated steam drying, MC_{eq}, is approximated as (Hasibuan et al., 2007)

$$MC_{eq} = 15.365 \exp\left(-0.001(T_b - 100)^{1.869}\right) \Big/ 1 + \left(15.365 \exp\left(-0.001(T_b - 100)^{1.869}\right)\right) \quad (20)$$

where T_b is the bed (drying) temperature. The heat transfer from the heating tubes to the particles in the fluidized bed dryer, α_t, is estimated as

Table 3. Elemental analysis of EFBs and conditions of drying, gasification, and the combined cycle

Properties	Value
Elemental analysis	
C (wt.% db)	46.62
H (wt.% db)	6.45
N (wt.% db)	1.21
S (wt.% db)	0.035
O (wt.% db)	45.66
Drying conditions	
EFB diameter (mm)	5
Silica sand diameter (mm)	0.3
Minimum fluidization velocity (m s-1)	0.041
Bed side length and height (m)	5
Gasification conditions	
Temperature (°C)	800, 900, 1000
Particle size (mm)	0.3
Minimum syngas cooling temperature (°C)	600
Bed side length and height (m)	5
Combined cycle conditions	
Turbine inlet temperature (°C)	1300
Compressor outlet pressure (MPa)	2
Gas turbine adiabatic efficiency (%)	90
HRSG outlet pressure (MPa)	10
Steam turbine polytrophic efficiency (%)	90

Table 4. Effect of the gasification temperature on the produced syngas composition

Temperature (°C)	Gasification yield (wt%)	Gas product component (vol%)				LHV (MJ m−3)
		H2	CO	CH4	CO2	
800	68.24	17.23	33.35	11.74	37.68	11.86
900	80.05	27.42	33.08	14.29	25.21	13.84
1000	91.7	38.02	36.36	14.72	10.90	15.55

$$\frac{\alpha_t d_p}{\lambda_g} = 0.74\, Ar^{0.1}\left(\frac{\rho_p}{\rho_g}\right)^{0.14}\left(\frac{C_p}{C_g}\right)^{0.24}\upsilon_p^{2/3} + 0.46\, Re\, Pr\frac{\upsilon_p^{2/3}}{\upsilon_g} \tag{21}$$

where d_p, λ_g, Ar, ρ_p, ρ_g, C_p, C_g, υ_p, υ_g, and Pr are the particle diameter, gas thermal conductivity, particle density, gas density, particle specific heat capacity, gas specific heat capacity, particle volumetric fraction, gas volumetric fraction, and Prandtl number of the gas, respectively.

In addition, the heat transfer coefficient following the condensation of compressed steam inside the heating tubes, α_c, is estimated as

$$\alpha_c = \frac{0.023\, Re_l^{0.8}\, Pr_l^{0.4}\, \lambda_l}{d_t}\left[0.55 + 2.09/\Delta p_t^{0.38}\right] \tag{22}$$

where Re_l, Pr_l, λ_l, d_t, and p_t are the Reynolds number of the liquid, Prandtl number of the liquid, thermal conductivity of the liquid, tube inner diameter, and pressure inside the heating tubes, respectively.

Moreover, the heat transfer from the fluidizing medium (silica sand) to EFB particles, α_p, is approximated as

$$\alpha_p = 2.923 d_s^{-0.503} d_p^{-0.140} \tag{23}$$

where d_s and d_p are the average diameters of the EFB sample and particle (sand), respectively.

Figure 9 shows the simulation results of the proposed integrated-power generation from EFBs based on EPI versus the gasification temperature. The gasification temperature affects the produced syngas composition and the amount of exchanged heat in the cooler that preheats the steam before it is superheated in the HRSG. A higher gasification temperature leads to higher syngas conversion, higher LHV of syngas, and a larger amount of available heat to be recovered in the cooler. As the gasification temperature increases, the work generated by both gas and steam turbines increases. However, the work of the compressor also increases following the increase in gasification temperature owing to a larger amount of air required for combustion. However, the total net generated power is positive and notably increases following an increase in gasification temperature.

The total power generation efficiency in the case of a gasification temperature of 1000°C is 43.5%, which is considered to be high because the system also includes EFB drying. Hence, a gasification temperature of 1000°C is proposed as the optimal gasification temperature to achieve high total energy efficiency.

Figure 10 is a temperature–enthalpy diagram of the integrated power generation from EFBs including drying, gasification, and the combined cycle.

The solid and dotted lines represent the hot and cold streams, respectively. Generally, the hot and cold streams are almost parallel to each other, leading to effective heat coupling and minimum exergy destruction. In drying, the largest amount of heat exchange takes place in the fluidized bed dryer, where the condensation heat of compressed steam is exchanged with the evaporation heat of water from EFBs.

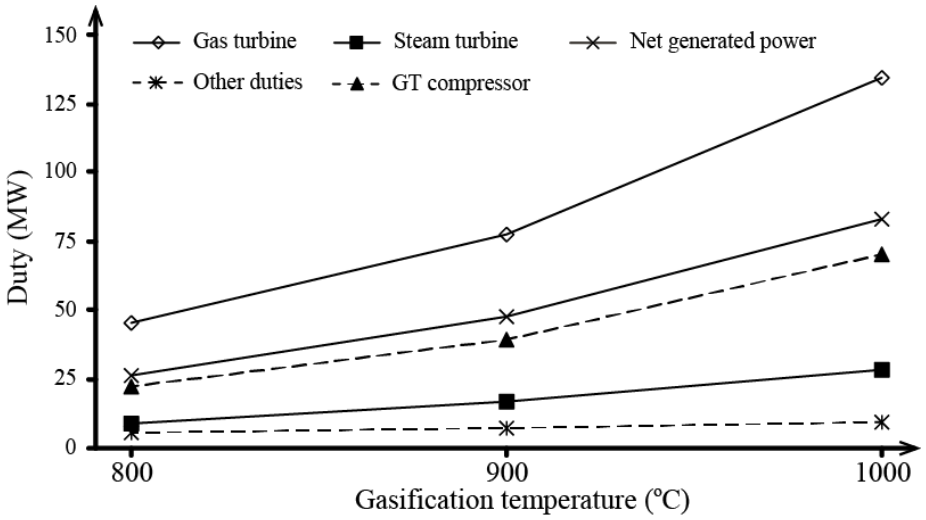

Figure 9. Simulation results of the integrated power generation from EFBs based on EPI versus the gasification temperature.

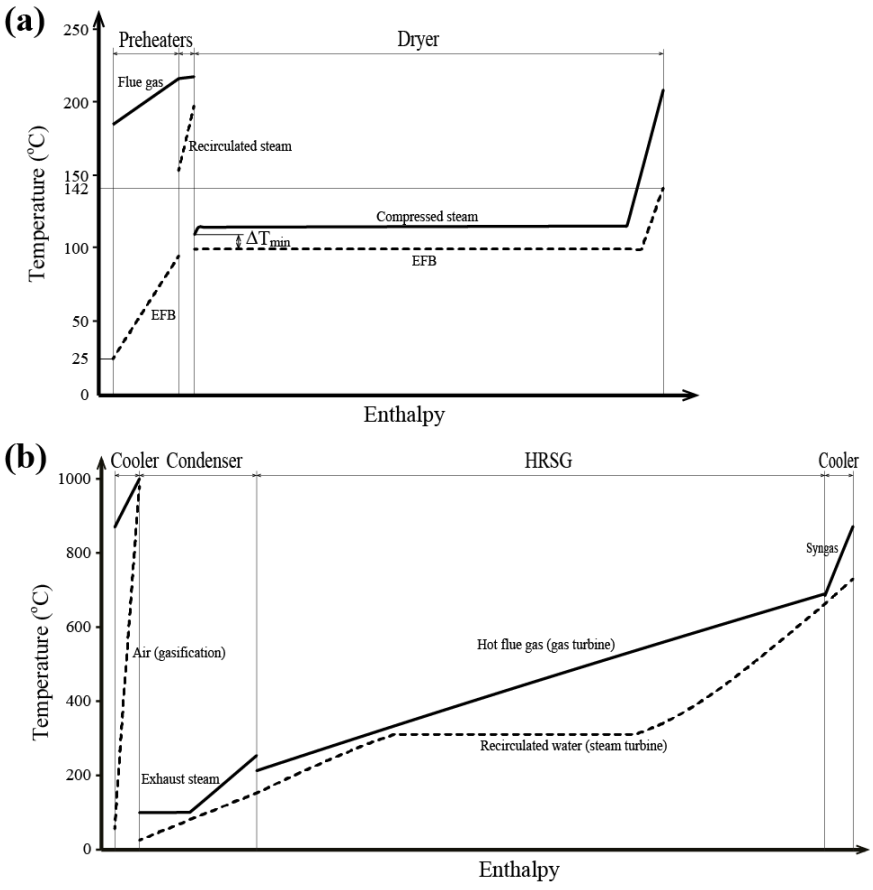

Figure 10. Temperature–enthalpy diagram of the integrated power generation from EFBs: (a) drying, (b) gasification and combined cycle (gasification temperature of 1000°C).

Through compression, the exergy rate of the cold stream is elevated, leading to the possibility of self-heat exchange.

In the gasification and combined cycle, the largest heat exchange occurs within the HRSG, where the exhaust gas from the gas turbine is recovered for steam generation. Because of the difference in material composition, the hot and cold streams inside the HRSG have different curves. In the cold stream, water is heated in a process involving both sensible and latent heat. Moreover, the air for gasification is preheated using the heat of produced syngas, and therefore the exergy destruction during gasification can be minimized.

CONCLUSION

EPI technology has been developed and applied in industrial processes, especially those related to energy harvesting. EPI comprising exergy recovery and process integration can improve the total energy efficiency of a system, although compared with currently available heat recovery technology. Exergy can be recovered through exergy elevation and effective heat coupling leading to the minimization of exergy destruction in a single process. In addition, the exergy destruction in the whole integrated processes can be minimized through the application of process integration.

Furthermore, EPI has been evaluated for the drying of LRC and integrated power generation from microalgae and EFBs. All modeled and evaluated processes show very high energy efficiency. The results will lead to further application in real industrial processes.

REFERENCES

Aziz, M., Kansha, Y., Tsutsumi, A., (2011). Self-heat recuperative fluidized bed drying of brown coal. *Chem. Eng. Process*, 50, 944-951.

Aziz, M., Kansha, Y., Kishimoto, A., Kotani, Y., Liu, Y., Tsutsumi, A., (2012a). Advanced energy saving in low rank coal drying based on self-heat recuperation technology. *Fuel Process. Technol.*, 104, 16-22.

Aziz M., Oda T., Kashiwagi T., (2012b). Enhanced high energy efficient steam drying of algae. *Appl. Energy*, 109, 163-170.

Aziz M., Oda T, Kashiwagi T., (2014a). Integration of energy-efficient drying in microalgae utilization based on enhanced process integration. *Energy*, 70, 307-316.

Aziz M., Oda T., Kashiwagi T., (2014b). Energy-efficient low rank coal drying based on enhanced vapor recompression technology. *Drying Technol*., 32, 1621-1631.

Aziz M., Oda T., Kashiwagi T., (2014c). Advanced energy harvesting from algae—Innovative integration of drying, gasification and combined cycle. *Energies*, 7, 8217-8235.

Aziz, M., (2015a). Integrated supercritical water gasification and a combined cycle for microalgal utilization. *Energy Convers. Manage.*, 91, 140-148.

Aziz, M., Prawisudha, P., Prabowo, B., Budiman, B. A., (2015b). Integration of energy-efficient empty fruit bunch drying with gasification/combined cycle systems. *Appl. Energy*, 139, 188-195.

Aziz, M., Oda, T., Kashiwagi, T., (2015c). Design and analysis of energy-efficient integrated crude palm oil and palm kernel oil processes. *J. Jpn. Inst. Energy*, 94, 143-150.

Chaiwong, K., Kiatsiriroat, T., Vorayos, N., Thararax, C., (2012). Biochar production from freshwater algae by slow pyrolysis. *Maejo Int. J. Sci. Technol.*, 6, 186-195.

Chakinala, A. G., Brilman, D. W. F., van Swaaij, W. P. M., Kersten, S. R. A., (2010). Catalytic and non-catalytic supercritical water gasification of microalgae and glycerol. *Ind. Eng. Chem. Res.*, 49, 1113–1122.

Chen, Z.; Agarwal, P. K.; Agnew, J. B., (2001). Steam drying of coal. Part 2. Modeling the operation of a fluidized bed drying unit. *Fuel*, 80, 209-223.

Devahastin, S., Mujumdar, A. S., (2007). Indirect dryers. In: Handbook of Industrial Drying; Mujumdar, A. S. Ed.; CRC Press: Boca Raton, 137-149.

Haiduc, A. C., Branderberger, M., Suquet, S., Vogel, F., Bernier-Latmani, R., Ludwig, C., (2009). SunCHem: an integrated process for the hydrothermal production of methane from microalgae and CO2 mitigation. *J. Appl. Phycol.*, 21, 529-541.

Hasibuan, R., Wan Daud, W. R., (2007). Through drying characteristic of oil palm empty fruit bunch (EFB) fibers using superheated steam. *Asia-Pac. J. of Chem. Eng*., 2, 35-40.

Hu, S., Man, C., Gao, X., Zhang, J., Xu, X., Che, D., (2013). Energy analysis of low-rank coal pre-drying power generation systems. *Drying Technol.*, 31, 1194-1205.

Hu, Z., Ma, X., Li, L., Wu, J., (2014). The catalytic of microalgae to produce syngas. *Energy Convers. Manage.*, 85, 545-550.

Kerdsuwan, S., Laohalidanond, K., (2011). Renewable energy from palm oil empty fruit bunch. In: Nayeripour M, editor. *Renewable energy–trends and applications*, Rijeka: InTech Open; pp. 123–50.

Kotani, Y., Aziz, M., Kansha, Y., Fushimi, C., Tsutsumi, A., (2013). Magnetocaloric heat circulator based on self-heat recuperation technology. *Chem. Eng. Sci*., 101, 5-12.

Kruse, A., (2008). Review: supercritical water gasification. *Biofuels. Bioprod. Biorefin.*, 2, 415–437.

Liu, Y., Aziz, M., Kansha, Y., Tsutsumi, A., (2012a). Drying energy saving by applying self-heat recuperation technology to biomass drying system. *Chem. Eng. Trans.*, 29, 577-582.

Liu, Y., Aziz, M., Fushimi, C., Kansha, Y., Mochidzuki, K., Kaneko, S., Tsutsumi, A., Yokohama, K., Myoyo, K., Oura, K., Matsuo, K., Sawa, S., Shinoda, K., (2012b). Exergy analysis of biomass drying based on self-heat recuperation technology and its application for industry: a simulation and experimental study. *Ind. Eng. Chem. Res.*, 51, 9997−10007.

Liu, Y., Aziz, M., Kansha, Y., Tsutsumi, A., (2013). A Novel exergy recuperative drying module and its application for energy-saving drying with superheated steam. *Chem. Eng. Sci.*, 100, 392-401.

Liu, Y., Aziz, M., Kansha, Y., Tsutsumi, A., (2014). Application of the self-heat recuperation technology for energy saving in biomass drying system. *Fuel Process. Technol*., 117, 66-74.

Lu, Y., Zhao, L., Han, Q., Wei, L., Zhang, X., Guo, L., Wei, J., (2013). Minimum fluidization velocities for supercritical water fluidized bed within the range of 633-693 K and 23 -27 MPa. *Int. J. Multiphase Flow*, 49, 78-82.

Matsumura, Y., Minowa, T., (2004). Fundamental design of a continuous biomass gasification process using a supercritical water fluidized bed. *Int. J. Hydrogen Energy*, 29, 701-707.

McGinn, P. J., Dickinson, K. E., Bhatti, S., Frigon, J. C., Guiot, S. R., O'Leary, S. J. B., (2011). Integration of microalgae cultivation with industrial waste remediation for biofuel and bioenergy production: opportunities and limitations. *Photosynth. Res.*, 109, 231-247.

Mohammed, M. A. A., Salmiaton, A., Wan Azlina, W. A. K. G., Mohamad Amran, M. S., (2011). Gasification of empty fruit bunch for hydrogen rich fuel gas production. *J. Appl. Sci*., 11, 2416–2420.

Mohammed, M. A. A., Salmiaton, A., Wan Azlina, W. A. K. G., Mohammad Amran, M.S., (2012). Gasification of oil palm empty fruit bunches: A characterization and kinetic study. *Bioresour. Technol.*, 110, 628–36.

O-Thong, S., Boe, K., Angelidaki, I., (2011). Thermophilic anaerobic co-digestion of oil palm empty fruit bunches with palm oil mill effluent for efficient biogas production. *Appl. Energy*, 93, 648-654.

Paepatung, N., Nopharatana, A., Songkasiri, W., (2009). Bio-methane potential of biological solid materials and agricultural wastes. *Asian J. Energy Env.*, 10: 19–27.

Ventikasamy, C., Hendry, D., Wilkinson, N., Fernando, L., Jacoby, W. A., (2011). Investigation of thermochemical conversion of biomass in supercritical water using batch reactor. *Fuel*, 90, 2662-2670.

Zhu, F. X. X., (2014). Energy and Process Optimization for the Process Industries. New Jersey: John Wiley & Sons, 2014.